Intraseasonal impact of the Scandinavian pattern on winter surface air temperature over Asia

Qilei Huang

1756525575@qq.com

Nanjing University of Information Science and Technology

Ning Shi

Nanjing University of Information Science and Technology https://orcid.org/0000-0002-4769-1609

Botao Zhou

Nanjing University of Information Science and Technology

Research Article

Keywords: Scandinavian pattern, Eastern China, Intraseasonal impact, Surface air temperature, PV inversion

Posted Date: January 30th, 2024

DOI: https://doi.org/10.21203/rs.3.rs-3877222/v1

Abstract

This study employs the ERA5 and JRA55 monthly reanalysis datasets to examine the intraseasonal impact of the Scandinavian (SCA) teleconnection pattern on the surface air temperature (SAT) over Asia in boreal winters from 1958 to 2021. We demonstrate that the impacts of the SCA pattern exhibit evident intraseasonal variations. Notably, the accumulated SAT anomalies over the region to the north of Tibetan Plateau (NP) due to the SCA pattern tend to propagate southward to the eastern China (EC) during late winter, which is associated with the gradually intensifying westward gradient of the air temperature to the east of Tibetan Plateau. Furthermore, both the November and January SCA patterns can significantly cause one-month-lagged SAT anomalies over the NP, albeit through different mechanisms. For the November SCA pattern, the associated snow cover anomalies can persist until December, facilitating the formation of local significant SAT anomalies via anomalous sensible heat flux. In contrast, from January to February, the background gradients of both the air temperature and potential vorticity intensify, creating more favorable conditions for the vertical coupling between the upper and lower circulation anomalies associated with the SCA pattern. Consequently, the SCA pattern tends to persist, leading to significant SAT anomalies over both the NP and EC in February. These significant influences of the SCA pattern exhibit evident interdecadal variations.

1. Introduction

Wallace and Gutzler (1981) proposed that there are generally five teleconnection patterns during the boreal winter in the Northern Hemisphere. Among these patterns, the Eurasian (EU) teleconnection pattern holds an important position as it arises over the extensive Eurasian continent and significantly influences the local weather and climate. Subsequently, Barnston and Livezey (1987) applied the rotated principal component analysis method to further classify the EU teleconnection pattern into two types: EU type 1 and EU type 2. For the EU type 1, one of its primary anomaly centers is located around the Scandinavian Peninsula and, thus, it has been named the Scandinavian (SCA) pattern by the Climate Prediction Center/National Oceanic and Atmospheric Administration (CPC/NOAA) of the United States. The two other primary anomaly centers of the SCA are located approximately over the Atlantic/Europe and to the southwest of Lake Baikal, respectively. Overall, these three primary anomaly centers exhibit an arc-shaped circulation structure over the Eurasian continent.

Bueh and Nakamura (2007) initially found that the three anomaly centers of SCA pattern are formed and maintained via different dynamic processes. Specifically, the Atlantic/European center is maintained mainly through feedback forcing from high-frequency transient eddies. Meanwhile, the center around Lake Baikal is related mainly to the propagation of low-frequency Rossby wave packets. Finally, the center around the Scandinavian Peninsula is formed by the combined effects of the abovementioned high-frequency and low-frequency dynamics. In the vertical direction, Zhang et al. (2022) noted that there is a vertical coupling effect between upper tropospheric circulation anomalies and SAT anomalies over the mid- and high-latitude Eurasia during the evolution of the SCA events. This vertical coupling effect is similar to that between the wave train anomalies across the Eurasian continent and SAT anomalies over

mid-latitude Asia, as proposed by Takaya and Nakamura (2005). The vertical coupling effect facilitates the persistence of the SCA pattern. In addition, Wang and Tan (2020) found that the anomalous convective activity over the North Atlantic may facilitate the sustenance of the SCA pattern on the intraseasonal timescales.

Several studies have demonstrated that the SCA pattern mainly influences the SAT in the mid- and high-latitude Eurasia. Taking the positive phase of the SCA pattern as an example, the primary anticyclonic center around the Scandinavian Peninsula and the cyclonic center near Lake Baikal usually correspond to a large-scale southwest-northeast tilted ridge and a trough over the Eurasian continent, respectively (Bueh et al. 2011; Peng and Bueh 2012). Such anomalous circulation is a precursory atmospheric signal for the enhanced Siberian high (Takaya and Nakamura 2005; Song et al. 2023). These anomalous circulation systems can induce anomalous southward advection of cold air masses from the high latitudes, and can lead to the formation of negative surface air temperature (SAT) anomalies near the region from Lake Balkhash to Lake Baikal (Bueh and Nakamura 2007).

Theoretically, once the SAT anomalies form and accumulate in the middle and high latitudes of the Eurasian continent, they tend to propagate southeastward as surface thermal Rossby waves along climatological mean potential temperature contours in the northwest-southeast direction (Fig. 1). Accordingly, East Asia is usually subject to the southeastward intrusion of cold air masses (Hu et al. 2005; Yang and Li 2016). Under such circumstances, the influence of the SCA pattern can extend to the middle and lower latitudes. For example, Zhu and Chen (2019) found that the positive phase of the SCA pattern is significantly associated with increased snowfall in the Yangtze-Huaihe River Basin of China due to the strengthened cold-air activity and intensified water vapour transport. Compared to the short-lived cold surges, the SCA pattern is more favorable for the formation of long-lasting cold surges over the South China Sea (Pang et al. 2022). Furthermore, after systematically comparing the intraseasonal impacts of the major teleconnection patterns in the Northern Hemisphere during the boreal winter, Shi et al. (2019) discovered that the SCA pattern is the only teleconnection pattern that can significantly and persistently affect the SAT over eastern China during the period from one to two weeks after the peak day of the SCA pattern. Such an extremely lagged impact of the SCA pattern is associated with the vertical coupling effect between the upper circulation anomalies and SAT anomalies and with the diabatic heating anomalies over the Eurasian continent (Zhang et al. 2022).

Considering the fact that the cold air masses may gradually propagate southward, we speculate that on the monthly mean timescales, the SCA pattern may also exert a significant influence on the SAT over East Asia if the SCA pattern is dominant or occurs frequently in a particular month. Although Bueh and Nakamura (2007) showed that the January SCA can hardly induce significant SAT over East Asia (their Fig. 9b), the presence of the extremely lagged influence of the SCA pattern (Shi et al. 2019; Zhang et al. 2022) implies that the monthly influence of the SCA pattern has an intraseasonal variation. Note that previous studies have demonstrated that some particular circulation anomalies or systems have intraseasonal variations in their influences on East Asia, e.g., the Arctic Oscillation (Ting and Peng 1995; Qiao and Feng 2016; Geng et al. 2017) and stratospheric polar vortex (Yan et al. 2022). The intraseasonal

influences of the Arctic Oscillation or stratospheric polar vortex may be associated with their phase shifts. In contrast, the present study mainly focuses on the impact of intraseasonal variations on the SCA under the condition that its phase remains unchanged. Clearly, our study differs from these previous studies.

Motivated by the above-mentioned studies and to better understand weather and climate anomalies over Asia, it is meaningful for further discussion on the intraseasonal influences of the SCA pattern, especially the lagged influences. To this end, the paper is organized as follows. Section 2 provides a description of the dataset and analysis methods used in this study. In Section 3, we present the statistical relationship between the SCA pattern and SAT anomalies over eastern China, and the reasons for the monthly relationship between the SCA pattern and the SAT over eastern China. The final section presents the main conclusion and discussion.

2. Data and Methods

To obtain robust and reliable results, two monthly reanalysis datasets are utilized in the present study. One dataset is derived from the latest generation reanalysis dataset ERA5 provided by the European Centre for Medium-Range Weather Forecasts (Hersbach et al. 2020); the other dataset is from the JRA55 reanalysis dataset produced by the Japan Meteorological Agency (Kobayashi et al. 2015). The present study mainly shows the results derived from the ERA5 reanalysis dataset, while the results from the JRA55 reanalysis dataset are provided in the supplementary material. The period spanning from 1958 to 2021 is analysed, which covers the extended winter season from November to March of the next year. The primary variables utilized include the geopotential height, air temperature, SAT, wind velocity, snow cover, snowfall, and surface sensible heat flux. The monthly anomalies are obtained by subtracting the climatological mean from the corresponding monthly data. For a particular calendar month, its climatological mean is taken as the mean of the monthly data for the corresponding month from 1979 to 2018. In fact, to check the sensitivity of the final results to the choice of climatological mean period, we also take the climatological mean from 1958 to 2021, and the final results are not qualitatively changed.

The spatial structure of the SCA pattern and its monthly index are calculated using the methods of Barnston and Livezey (1987) and the CPC/NOAA. First, the empirical orthogonal function (EOF) is applied to the standardized 500 hPa geopotential height anomalies for five boreal winter months from 1979 to 2018 (40 years × 5 months/year = 200 months). Second, the first ten modes are subjected to rotated EOF analysis (REOF), and the eighth mode in ERA5 or the sixth mode in JRA55 is recognized as the SCA pattern. Finally, the standardized 500 hPa geopotential height anomalies for each winter month from 1958 to 2021 are projected onto the SCA pattern, and the resulting time series are standardized and referred to as the monthly SCA index.

To analyse the reason for the persistence of the SCA, potential vorticity (PV) inversion is applied (Davis et al. 1992; Takaya and Nakamura 2005). In the quasigeostrophic framework, PV anomaly is defined as

$$q' = L_g(\varphi')$$

1

,

where $L_g = \nabla^2 + {f_0}^2 \partial(1/\sigma \cdot \partial/\partial p)\partial p$ is the Laplace operator and superscript is the anomaly; $\varphi' = \phi'/f_0$ is the geostrophic streamfunction anomaly; ϕ' is the geopotential anomaly; f_0 is set to 1e-4 s^{-1}; $\sigma = -(\alpha/\theta)(\partial\theta/\partial p)$ is the static stability, which is taken as the climatological mean north of 40°N; α is the specific volume; and θ is the potential temperature. Under adiabatic and frictionless conditions, PV is characterized by its conservation and invertibility. The boundary conditions are Neumann boundary conditions:

$$\frac{\partial \varphi'}{\partial p} = -\frac{R\theta'}{f_0 p}\left(\frac{p}{p_0}\right)^{\frac{R}{c_p}}$$

2

,

which is applied at both 1000 hPa and 100 hPa. Given the distribution of q' and appropriate boundary conditions, L_g can be inverted for the φ' distribution, i.e., $\varphi' = {L_g}^{-1}(q')$. Via this PV inversion method, we can measure the coupling effect of upper and lower tropospheric circulation anomalies associated with the SCA.

3. Results

Figure 2a shows the positive phase of the SCA pattern, which is represented as the regression of 500 hPa geopotential height anomalies onto the standardized monthly SCA indices from 1979 to 2018. Obviously, it is characterized by a primary anticyclonic anomaly center around the Scandinavian Peninsula, and two cyclonic anomaly centers around northern Africa and Lake Baikal, respectively. The typical influence of the SCA pattern on the SAT is represented by the simultaneous regression coefficients of monthly SAT anomalies onto the normalized SCA indices (Fig. 2b). Significant negative SAT anomalies are observed over almost the whole middle and high latitudes of the Eurasian continent. In addition, the negative SAT anomalies extend southeastward along the Tibetan Plateau from central Siberia to eastern China. Accordingly, we choose two areas as the key regions to further discuss the intraseasonal influences of the SCA pattern. One is the region to the north of Tibetan Plateau (45–60°N, 70–110°E), which is referred to as the NP and is indicated by the solid black rectangle in Fig. 2. This region is often regarded as the key region for cold surge occurrence by Chinese meteorologists. The other region is the eastern China (25–40°N, 110–120°E), which is referred to as EC and is indicated by the solid orange rectangle.

a. Simultaneous influence

Table 1 shows the simultaneous and one-month lead-lag correlation coefficients between the monthly SCA index and regional averaged SAT anomalies. The underlined values indicate that both the ERA5 and JRA55 datasets show consistent results in terms of the significance of the correlation coefficients at least

at the 95% confidence level. Evidently, the SCA index has significant simultaneous correlation coefficients with SAT anomalies over the NP in all winter months. Over the 64-year period from 1958 to 2021, these correlation coefficients are consistently above − 0.76, which passes the 99% confidence level. The maximum value reaches as high as -0.81 which occurs in March. This indicates that the SCA pattern facilitates the accumulation and maintenance of cold air masses over the NP, which is associated with the southward cold advection by the anticyclonic anomaly centred around the Scandinavian Peninsula (Zhang et al. 2022). In contrast, the simultaneous relationships between the SCA index and SAT anomalies over EC show evident intraseasonal differences. In the early winter months, there is no significant relationship between them. Thus, these findings are consistent with the findings of Bueh and Nakamura (2007) that the SCA does not exert significant influence over the EC in January. However, in the later winter months, i.e., February and March, the correlation coefficients notably increase to approximately − 0.43, passing the 99% confidence level.

Table 1
Correlation coefficients between monthly SCA indices and regional mean SAT anomalies over the NP (45–60°N, 70–110°E) and EC (25–40°N, 110–120°E) regions from 1958 to 2021 according to the ERA5 dataset. One-month auto lead-lag correlation coefficients are also shown in the last row. ** and * indicate significance at the 99% and 95% confidence levels, respectively. Underlined values indicate that the correlation coefficients are also significant at the 95% confidence level by the JRA55 dataset

		SCA Indices				
		November	**December**	**January**	**February**	**March**
Regional SAT	**Simultaneous NP**	-0.78**	-0.71**	-0.76**	-0.80**	-0.81**
	Simultaneous EC	-0.14	-0.02	-0.11	-0.43**	-0.44**
	next month NP	-0.39**	-0.25*	-0.47**	-0.20	-0.27*
	next month EC	-0.13	-0.10	-0.34**	-0.24	-0.21
SCA Indices	**next month**	0.19	0.25*	0.32**	0.07	0.09

In fact, the circulation anomalies in the middle and upper troposphere associated with the SCA pattern show no evident difference in different winter months (not shown). The above-mentioned intraseasonal variation may be caused by the difference in the background gradient of air temperature or potential temperature in the lower troposphere. To discuss this issue, Fig. 3 shows the zonal gradient of air temperature at the lowest atmospheric levels in the region to the east of Tibetan Plateau (designated by the red box area in Fig. 1). This region is just to the southeast of the NP where significant SAT anomalies

occur (Fig. 2b). The larger the value of the gradient is, the easier the air temperature anomalies propagate southward from the NP to the EC. As shown in Fig. 3, the average zonal gradient generally amplifies from early winter to late winter in the lower troposphere. Note that there is an evident amplification from January to February in the lower troposphere (except at 925 hPa, for which the most evident amplification occurs from December to January). The gradient reaches its maximum values in March and then gradually diminishes after April (not shown). This intraseasonal variation in the zonal gradient can be verified by the JRA55 dataset (Fig. S1). The enhanced zonal temperature gradient during late winter means that it is easier for the air temperature anomaly to invade southward into the EC as thermal Rossby waves during late winter. In other words, the variation in the background low-level temperature gradient accounts for the evident intraseasonal variation in the relationship between the SCA index and SAT anomalies over EC.

b. Lagged impact of the SCA

Regarding the lagged impact of the SCA pattern, Table 1 shows that the one-month lagged influence on the SAT is significant only in some particular months, exhibiting an evident month-to-month variation. The two-month lagged influences are not significant and, thus, are not shown here. According to the ERA5 dataset, the SCA indices overall exhibit a significant relationship with the one-month lagged SAT anomalies over the NP, except for the SCA in February. The correlation coefficients achieve local maximum values in November (-0.39) and January (-0.47). Unambiguously, the SCA pattern, especially in the early and mid-winter months can still induce significant SAT anomalies over the NP in the following one month. In contrast, only the January SCA pattern can induce significant SAT anomalies over the EC in the following one month, with a correlation coefficient of -0.34, passing the 99% confidence level. Such a significant relationship might be associated with the increased westward gradient of air temperature to the east of Tibetan Plateau in the later winter (Fig. 3), which induces the southward propagation of cold air masses from the NP. The JRA55 dataset shows basically consistent results, but it demonstrates that only the November and January SCA patten can induce the significant one-month-lagged influences over the NP, which are indicated by the underlines in Table 1. Moreover, these findings suggest suggests that the SCA pattern during the late winter months can induce significant one-month-lagged influences over the EC (not shown). Based on the consistent results from the two reanalysis datasets, the following text will explore the reasons for the significant influence of (1) the November SCA pattern on the NP and (2) the January SCA pattern on both the NP and EC.

First, the significant lagged influence of the November SCA pattern might be associated with snow cover. As revealed by previous studies (Yuan and Li 2019; Guan et al. 2020), increased snow cover over Siberia can persist through December to February, which facilitates the continuous southward intrusion of cold air into China and even the occurrence of extreme cold events. Climatologically, the northern part of the NP (approximately north of 50°N) is characterized by a large fraction of snow cover, while its southern part (approximately south of 50°N) has a small fraction ranging from 20–60% (shading in Fig. 1). The snow cover over the southern part of the NP is generally characterized by large variability and it might be an important factor for the lagged influence of the SCA. To explore this issue further, Fig. 4a displays the

simultaneous regression coefficients of the November snowfall anomalies onto the SCA index. November is distinct among all five winter months. In November, the SCA pattern can induce significant above-normal snowfall anomalies over the western NP, i.e., around Lake Balkhash (Fig. 4a). Consistently, the snow cover anomalies simultaneously increase (Fig. 4b) and persist until December (Fig. 4c). As a result, there are anomalously downward surface sensible heat flux over the western NP (Fig. 4d), contributing to the formation of significant cold SAT anomalies (Fig. 4e).

Second, the significant lagged influence of the January SCA pattern can be attributed to the persistence of the SCA pattern. The two reanalysis datasets consistently reveal that the SCA pattern tends to persist in the mid-winter (last row of Table 1). Specifically, the autocorrelation coefficient for the SCA indices between January and February is 0.32, which passes the significance at the 95% confidence level. Figure 5a shows the regression coefficients of the February geopotential height at 300 hPa onto the January SCA index. Evidently, there are still wave-like anomalies from Western Europe to Siberia in the upper atmosphere, resembling to the typical SCA pattern (Fig. 2a) except for their slightly eastward displacement. Such a persistence of the SCA pattern accounts for its lagged significant influence on the February SAT over the NP. Moreover, with the aid of the enhanced westward gradient of the air temperature during the late winter, the EC in February is also subject to the significant negative SAT anomalies (Fig. 5b). Note that snowfall does not seem to contribute to the formation of the lagged influence of the January SCA pattern. Because there are almost no significant snowfall anomalies in January (Fig. S2a) and no significant snow cover anomalies in February (Fig. S2b) over the NP. Therefore, there must be other processes responsible for the lagged influence of the January SCA pattern.

The persistence of the SCA pattern may be associated with the enhanced coupling effect. Takaya and Nakamura (2005) and Zhang et al. (2022) demonstrated that there is a vertical coupling effect between the upper- and lower-level atmospheric circulations. Importantly, the potential temperature gradient in the lower troposphere and potential vorticity gradient in the upper troposphere play essential roles in the vertical coupling effect. Motivated by these studies, Fig. 5c shows the difference in the climatological mean air temperature at 1000 hPa between February and January. On the one hand, due to the more rapid warming over the NP, the southward gradient of air temperature is enhanced overall around the Lake Baikal from January to February. Accordingly, strong southward cold air advection can be induced by the anomalous northerlies associated with the SCA pattern, which is favorable for the sustenance of cold anomalies over the NP in February, as shown in Fig. 5b. On the other hand, by performing piecewise PV inversion on the significant air temperature anomalies over the mid- and high-latitude Eurasia (40–60°N, 50–135°E), it can be seen that in the upper atmosphere a large-scale anticyclonic circulation anomaly occurs over the mid- and high-latitude Eurasia in February (Fig. 5d). The anomaly center is located to the west of Lake Baikal. Correspondingly, there are anomalous southerlies around the Ural Mountains (45–75°N, 30–65°E) and northerlies around Lake Baikal (40–75°N, 90–150°E). In terms of climatological mean PV at 300 hPa, it decreases evidently from January to February over the Ural Mountains and the region to the south of Lake Baikal. Thus, the negative PV advection is more easily be induced around the Ural Mountains, while positive PV advection is more easily be induced around Lake Baikal. Correspondingly, this process facilitates the maintenance of anticyclonic anomalies around Novaya

Zemlya and cyclonic anomalies around Lake Baikal (Fig. 5a). In fact, the above-mentioned changes in the climatological mean gradients of both PV and air temperature can hardly be observed in other months (Fig. S3). Therefore, although the circulation anomalies associated with the SCA pattern in a particular month generally diminish to a great extent from one month to the next month, the background fields change from January to February in such a way that they offer more favorable conditions for the vertical coupling between the upper-level circulation anomalies and SAT anomalies over the Eurasian continent, which facilitates the sustenance of the SCA pattern.

c. Interdecadal variation

To verify whether the influences of the SCA pattern vary with decades, Fig. 6 shows the 15-year running correlation coefficients between the monthly SCA index and the SAT anomalies over the EC and the NP in the boreal winter months. In fact, the results do not change qualitatively if the running window is set to 11 years. In terms of the simultaneous influences on the NP (Fig. 6a), all of the correlation coefficients pass the significance test at the 95% confidence level although the values of the coefficients vary to some extent. Thus, the SCA pattern can steadily cause significant negative SAT anomalies over the NP during the past decades. In contrast, the SCA pattern is influential for the EC SAT only in the late winter months and before the 2000s (Fig. 6c). The interdecadal variation can also be observed in the one-month lagged influence. Explicitly, only before the 1990s the November SCA pattern impacts the December SAT and the January SCA pattern impacts the February SAT over the NP (Fig. 6b). Interestingly, the influence of the January SCA pattern on the EC SAT has been gradually strengthening in recent decades since the coefficients become significant after the 2000s (Fig. 6d). The JRA55 reanalysis dataset shows quite similar results (Fig. S4). Therefore, when discussing the influences of the SCA pattern, it is essential to take into account its interdecadal effects.

4. Conclusion and Discussion

This study utilizes two reanalysis datasets, ERA5 and JRA55, to discuss the influence of the SCA pattern on the winter SAT over Asia and its intraseasonal variation. The results show that the SCA pattern can significantly lead to the formation of cold anomalies over the NP during each month of the boreal winter season. In contrast, the simultaneous impact of the SCA pattern on the SAT over the EC exhibits evident intraseasonal variations. The SCA pattern can influence the EC SAT only during the late winter months. This intraseasonal variation is associated with the strengthening of the westward gradient of the background potential temperature during the late boreal winter.

The SCA pattern also exhibits significant one-month-lagged influences in particular months. First, the November SCA index demonstrates a significant correlation relationship with the December SAT anomalies over the NP. This relationship may be attributed to the persistence of snow cover anomalies around Lake Balkhash. Second, the January SCA pattern can lead to substantial negative SAT anomalies in February across both the NP and the EC. The lagged influence is likely associated with intensified gradients of both the background potential vorticity in the upper troposphere and the background air

temperature in the lower troposphere. Such variations in the background field create more favorable conditions for vertical coupling between the upper troposphere circulation anomalies and the SAT anomalies, thereby facilitating the persistence of the January SCA pattern into February.

In recent decades, the escalating intensity of global warming has precipitated profound transformations in climate systems, resulting in a heightened incidence of extreme weather and climate events (Schär et al. 2016; IPCC 2021; Zandalinas et al. 2021; Zhang et al. 2021). To check the sensitivity of the results from Table 1 to global warming, we removed the long-term linear trend from 1958 to 2022 in each variable field and re-calculated Table 1 (shown in Table S1). Obviously, the final results are not qualitatively changed. Therefore, we can conclude that at least the long-term trend does not evidently change the intraseasonal variation in the SCA pattern.

There are two issues that require further investigation. First, the two reanalysis datasets fail to consistently demonstrate the one-month-lagged influence of the SCA pattern in February and March. Only the JRA55 reanalysis dataset exhibits a moderately significant influence on the SCA pattern over the EC during late winter (not shown). This discrepancy between the two reanalysis datasets necessitates further study. Second, the underlying mechanisms driving the interdecadal variations of the SCA influences remain uncertain. Our preliminary work suggests that neither changes in snow cover nor fluctuations in background gradients seem to be the fundamental factors responsible for these variations. Some studies have pointed out that several teleconnection patterns exhibit distinct interdecadal variations, such as the North Atlantic Oscillation which experienced a clear eastward shift in its activity center after 1976 (Hilmer and Jung 2000; Lu and Greatbatch 2002; Jung et al. 2003). Similarly, the Pacific/North American pattern transitioned from weak to strong approximately 1976, accompanied by an eastward shift (Lee et al. 2012). Motivated by these studies, we will further explore this issue by examining interdecadal variations in the morphology and intensity of the SCA pattern, as well as external forcings such as sea surface temperature and snow ice.

Declarations

Funding This work is jointly supported by the National Natural Science Foundation of China (No. 42025502 and 41975063).

Competing Interests The authors declare that they have no relevant financial or nonfinancial interests.

Author Contributions All the authors contributed to the study conception and design. Data collection, calculations, plot drawing and analysis were performed by Qilei Huang and Ning Shi. The first draft of the manuscript was written by Qilei Huang, and all the authors reviewed and edited previous versions of the manuscript. All the authors have read and approved the final manuscript.

Data Availability The ERA5 reanalysis data are available at https://cds.climate.copernicus.eu/cdsapp#!/dataset/reanalysis-era5-pressure-levels-monthly means?tab=form. The JRA55 reanalysis data are available through the National Center for Atmospheric Research

(USA): https://rda.ucar.edu/datasets/ds628.0/. Figures were drawn using the National Center for Atmospheric Research NCAR Command Language (NCL) Version 6.6.2, which is available at http://www.ncl.ucar.edu/.

References

1. Barnston A G and Livezey R E (1987) Classification, Seasonality and Persistence of Low-Frequency Atmospheric Circulation Patterns. Monthly Weather Review 115: 1083-1126. https://doi.org/10.1175/1520-0493(1987)115<1083:CSAPOL>2.0.CO;2
2. Bueh C and Nakamura H (2007) Scandinavian pattern and its climatic impact. Quarterly Journal of the Royal Meteorological Society 133: 2117-2131. https://doi.org/10.1002/qj.173
3. Bueh C, Fu X, and Xie Z (2011) Large-scale circulation features typical of wintertime extensive and persistent low temperature events in China. Atmospheric and Oceanic Science Letters 4: 235–241. https://doi.org/10.1080/16742834.2011.11446935
4. Davis C A (1992) Piecewise Potential Vorticity Inversion. Journal of Atmospheric Sciences 49: 1397-1411. https://doi.org/10.1175/1520-0469(1992)049<1397:PPVI>2.0.CO;2
5. Geng X, Zhang W, Stuecker M F, et al. (2017) Strong sub-seasonal wintertime cooling over East Asia and Northern Europe associated with super El Niño events. Scientific Reports 7: 3770. https://doi.org/10.1038/s41598-017-03977-2
6. Guan C, Yu L, Yan F, Zhang S (2020) Teleconnections between Snow Cover Change over Siberia and Crop Growth in Northeast China. Sustainability 12: 7632. https://doi.org/10.3390/su12187632
7. Hersbach H, Bell B, Berrisford P, et al. (2020) The ERA5 global reanalysis. Quarterly Journal of the Royal Meteorological Society 146: 1999-2049. https://doi.org/10.1002/qj.3803
8. Hilmer M and Jung T (2000) Evidence for a Recent Change in the Link Between the North Atlantic Oscillation and Arctic Sea Ice Export. Geophysical Research Letters 27: 989-992. https://doi.org/10.1029/1999GL010944
9. Hu Y, Tung K K, and Liu J (2005) A Closer Comparison of Early and Late-Winter Atmospheric Trends in the Northern Hemisphere. Journal of Climate 18: 3204-3216. https://doi.org/10.1175/JCLI3468.1
10. IPCC (2021) Climate Change 2021: The Physical Science Basis. Contribution of Working Group I to the Sixth Assessment Report of the Intergovernmental Panel on Climate Change [Masson-Delmotte V, Zhai P, Pirani A, et al.]. Cambridge University Press, Cambridge, United Kingdom and New York. https://doi.org/10.1017/9781009157896
11. Jung T, Hilmer M, Ruprecht E, et al. (2003) Characteristics of the Recent Eastward Shift of Interannual NAO Variability. Journal of Climate 16: 3371-3382. https://doi.org/10.1175/1520-0442(2003)016<3371:COTRES>2.0.CO;2
12. Kobayashi S, Ota Y, Harada Y, et al. (2015) The JRA-55 Reanalysis: General Specifications and Basic Characteristics. Journal of the Meteorological Society of Japan. Ser. II 93: 5-48. https://doi.org/10.2151/jmsj.2015-001

13. Lee Y Y, Kug J S, Lim G H, et al. (2012) Eastward Shift of the Pacific/North American Pattern On an Interdecadal Time Scale and an Associated Synoptic Eddy Feedback. International Jou rnal of Climatology 32: 1128-1134. https://doi.org/10.1002/joc.2329
14. Lu J and Greatbatch R J (2002) The Changing Relationship Between the NAO and Northern Hemisphere Climate Variability. Geophysical Research Letters 29: 51-52. https://doi.org/10.1029/2001GL014052
15. Pang B, Lu R, and Ren R (2022) Impact of the Scandinavian Pattern on Long-Lived Cold Surges over the South China Sea. Journal of Climate 35: 1773-1785. https://doi.org/10.1175/JCLI-D-21-0607.1
16. Peng B and Bueh C (2012) Precursory signals of extensive and persistent extreme cold events in China. Atmospheric and Oceanic Science Letters 5: 252-257. https://doi.org/10.1080/16742834.2012.11446999
17. Qiao S and Feng G (2016) Impact of the December north Atlantic oscillation on the following February East Asian trough. Journal of Geophysical Research 121: 10074-10088. https://doi.org/10.1002/2016JD025007
18. Shi N, Tian P, and Zhang L (2019) Simultaneous influence of the Southern Hemisphere annular mode on the atmospheric circulation of the Northern Hemisphere during the boreal winter. International Journal of Climatology 39: 2685-2696. https://doi.org/10.1002/joc.5981
19. Schär C, Ban N, Fischer E M, et al. (2016) Percentile indices for assessing changes in heavy precipitation events. Climatic Change 137: 201-216. https://doi.org/10.1007/s10584-016-1669-2
20. Song J, Shi N, and Huang Q (2023) Precursory atmospheric teleconnection patterns for strong Siberian High events. Atmospheric and Oceanic Science Letters 16: 19-23. https://doi.org/10.1016/j.aosl.2023.100376
21. Takaya K and Nakamura H (2005) Mechanisms of Intraseasonal Amplification of the Cold Siberian High. Journal of the Atmospheric Sciences 62: 4423-4440. https://doi.org/10.1175/JAS3629.1
22. Ting M and Peng S (1995) Dynamics of the early and middle winter atmospheric responses to the northwest Atlantic SST anomalies. Journal of Climate 8: 2239-2254. https://doi.org/10.1175/1520-0442(1995)008<2239:DOTEAM>2.0.CO;2
23. Wallace J M and Gutzler D S (1981) Teleconnections in the Geopotential Height Field during the Northern Hemisphere Winter. Monthly Weather Review 109: 784-812. https://doi.org/10.1175/1520-0493(1981)109<0784:TITGHF>2.0.CO;2
24. Wang M and Tan B (2020) Two Types of the Scandinavian Pattern: Their Formation Mechanisms and Climate Impacts. Journal of Climate 33: 2645-2661. https://doi.org/10.1175/JCLI-D-19-0447.1
25. Yan H, Yuan Y, Tan G, and Zi Y (2022) Possible impact of sudden stratospheric warming on the intraseasonal reversal of the temperature over East Asia in winter 2020/21. Atmospheric Research 268: 106016. https://doi.org/10.1016/j.atmosres.2022.106016
26. Yang S and Li T (2016) Intraseasonal variability of air temperature over the mid-high latitude Eurasia in boreal winter. Climate Dynamics 47: 2155-2175. https://doi.org/10.1007/s00382-015-2956-8

27. Yuan C and Li W (2019) Variations in the Frequency of Winter Extreme Cold Days in Northern China and Possible Causalities. Journal of Climate 32: 8127-8141. https://doi.org/10.1175/JCLI-D-18-0771.1
28. Zandalinas S I, Fritschi F B, and Mittler R (2021) Global Warming, Climate Change, and Environmental Pollution: Recipe for a Multifactorial Stress Combination Disaster. Trends in Plant Science 26: 588-599. https://doi.org/10.1016/j.tplants.2021.02.011
29. Zhang D, Shi N, and Tajie S (2022) Mechanisms of the subseasonal influences of Scandinavian events on winter surface air temperature over Eastern China. Atmospheric Research 268: 105994. https://doi.org/10.1016/j.atmosres.2021.105994
30. Zhang G, Zeng G, Yang X, and Jiang Z (2021) Future Changes in Extreme High Temperature over China at 1.5 ℃-5 ℃ Global Warming Based on CMIP6 Simulations. Advances in Atmospheric Sciences 38: 253-267. https://doi.org/10.1007/s00376-020-0182-8
31. Zhu L and Chen H (2019) Possible connection between anomalous activity of Scandinavian Atmospheric Teleconnection Pattern and winter snowfall in the Yangtze-Huaihe River Basin of China. Atmospheric and Oceanic Science Letters 12: 218-225. https://doi.org/10.1080/16742834.2019.1593041

Figures

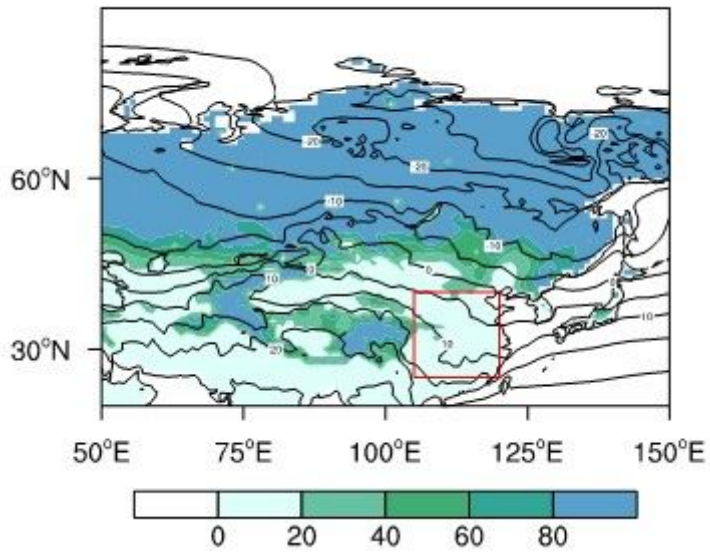

Figure 1

Climatological mean snow cover (shading; %) and 1000 hPa air temperature (contour; ℃) winters from November to March during the period from 1979 to 2018 (based on the ERA5 reanalysis dataset). The red rectangle represents the region (25-40°N, 105-120°E) used to calculate the averaged zonal gradient shown in **Fig. 3**

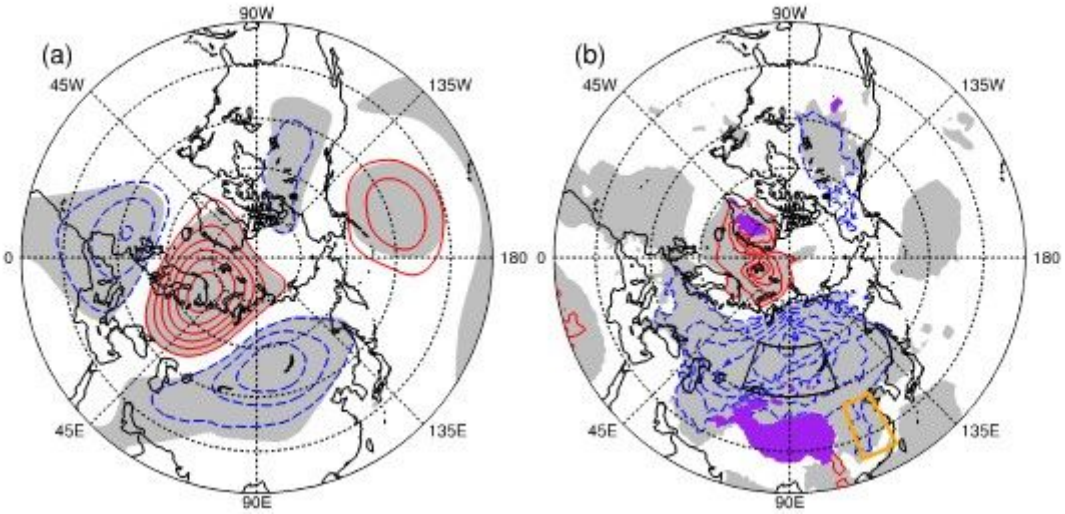

Figure 2

Monthly (a) 500 hPa geopotential height anomalies (unit: gpm, contour interval: 10 gpm) and (b) SAT anomalies (unit: ℃, contour interval: 0.5 ℃) regressed onto the normalized SCA indices from 1979 to 2018 (based on the ERA5 reanalysis dataset). Red solid lines represent positive anomalies, blue dashed lines represent negative anomalies, and zero lines have been omitted. Gray shading represents the significance at the 95% confidence level. In (b), purple shading represents terrain heights higher than 2500 m, the black rectangle represents the region to the north of Tibetan Plateau (45-60°N, 70-110°E) and the orange rectangle represents eastern China (25-40°N, 110-120°E) which are the focus of the following analysis

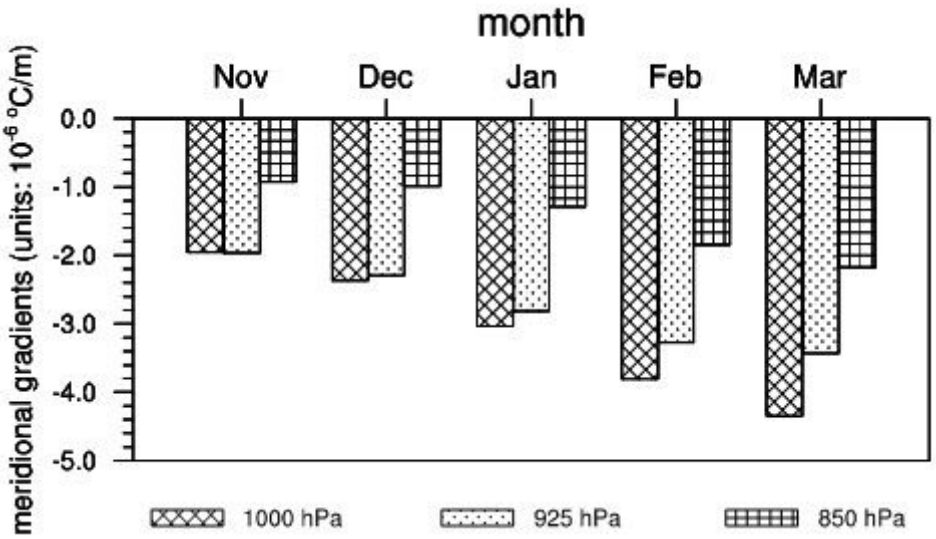

Figure 3

Averaged zonal gradients (10^{-6} ℃/m) of the climatological mean air temperature from 1979 to 2018 at 1000 hPa, 925 hPa, and 850 hPa in the region to the east of Tibetan Plateau (25-40°N, 105-120°E) (based on the ERA5 reanalysis dataset)

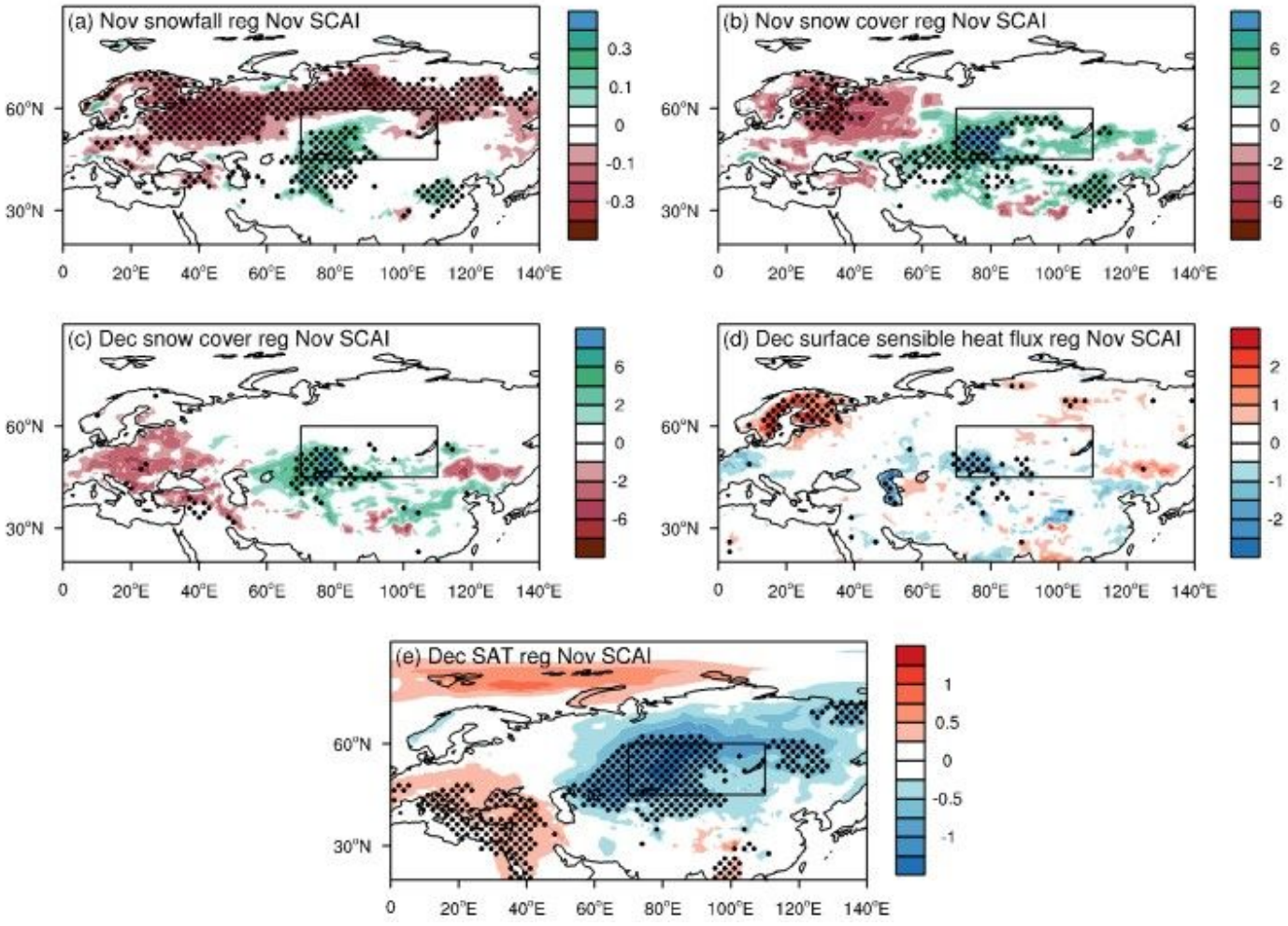

Figure 4

Regressed fields onto the November SCA indices from 1958 to 2021. (a) November snowfall anomalies (mm), (b) November snow cover anomalies (%), (c) December snow cover anomalies (%), (d) December surface sensible heat flux anomalies (W/m^2) and (e) December SAT anomalies (°C) (based on the ERA5 reanalysis dataset). The areas marked with black stippling indicate significance at the 95% confidence level. The black rectangle represents the NP (45-60°N, 70-110°E)

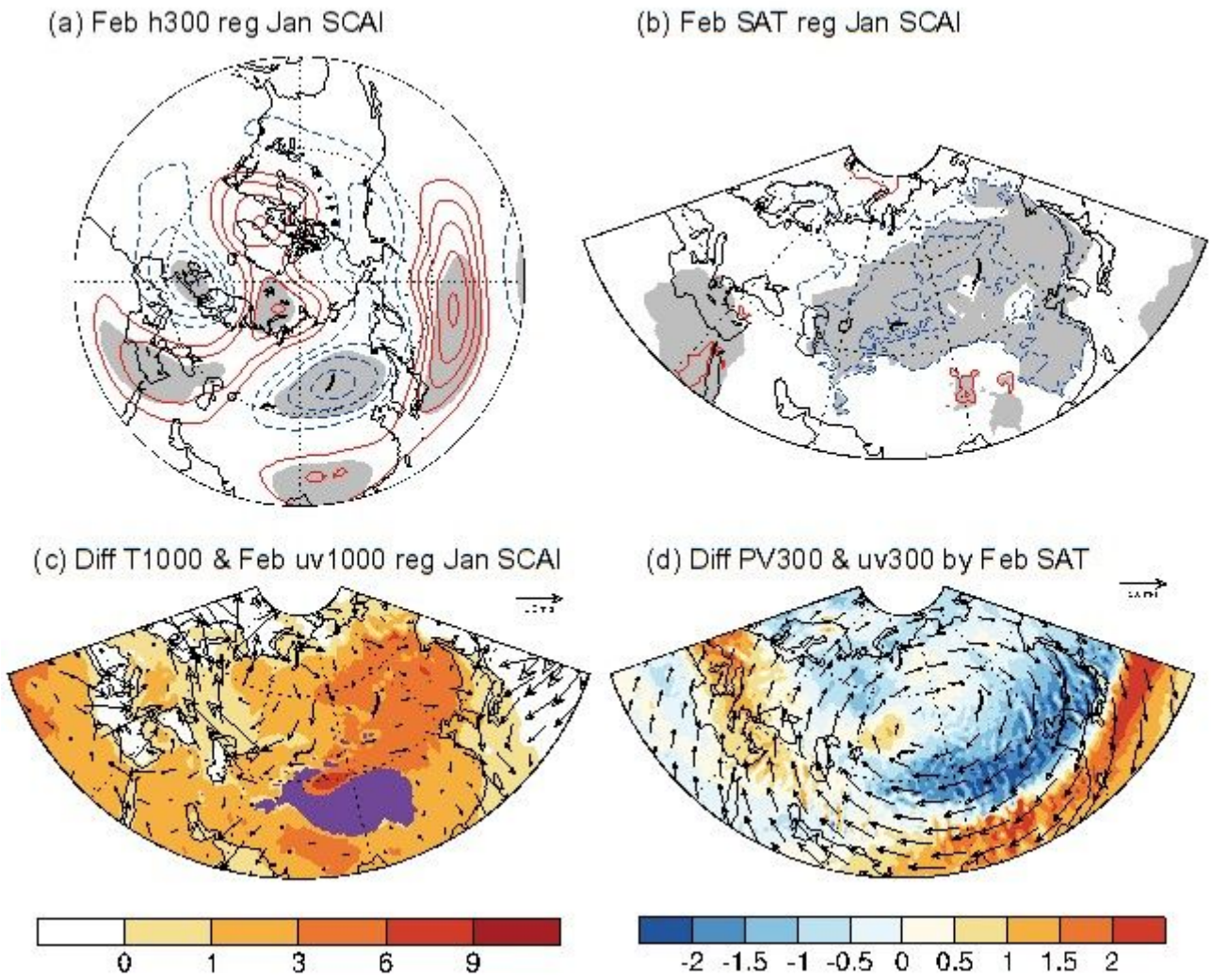

Figure 5

(a) February geopotential height anomalies (unit: gpm, contour interval: 10 gpm) at 300 hPa regressed onto the January SCA indices from 1958 to 2021; (b) February SAT anomalies (unit: ℃, contour interval: 0.5 ℃) regressed onto the January SCA indices; (c) difference in the climatological mean air temperature at 1000 hPa between February and January from 1979 to 2018 (shading; °C) and the regressed wind anomalies (m/s) at 1000 hPa in February onto the January SCA indices; (d) difference in the climatological mean PV at 300 hPa between February and January (shading; 10^{-5}/s), and 300 hPa wind anomalies (m/s) inverted from the negative SAT anomalies over the Eurasian continent (40-60°N, 50-135°E) in (b) (based on the ERA5 reanalysis dataset). Red solid lines and blue dashed lines represent positive and negative anomalies, respectively, with the zero lines omitted, and gray shading indicates significance at the 95% confidence level. In (c), purple shading represents terrain heights higher than 2500 m

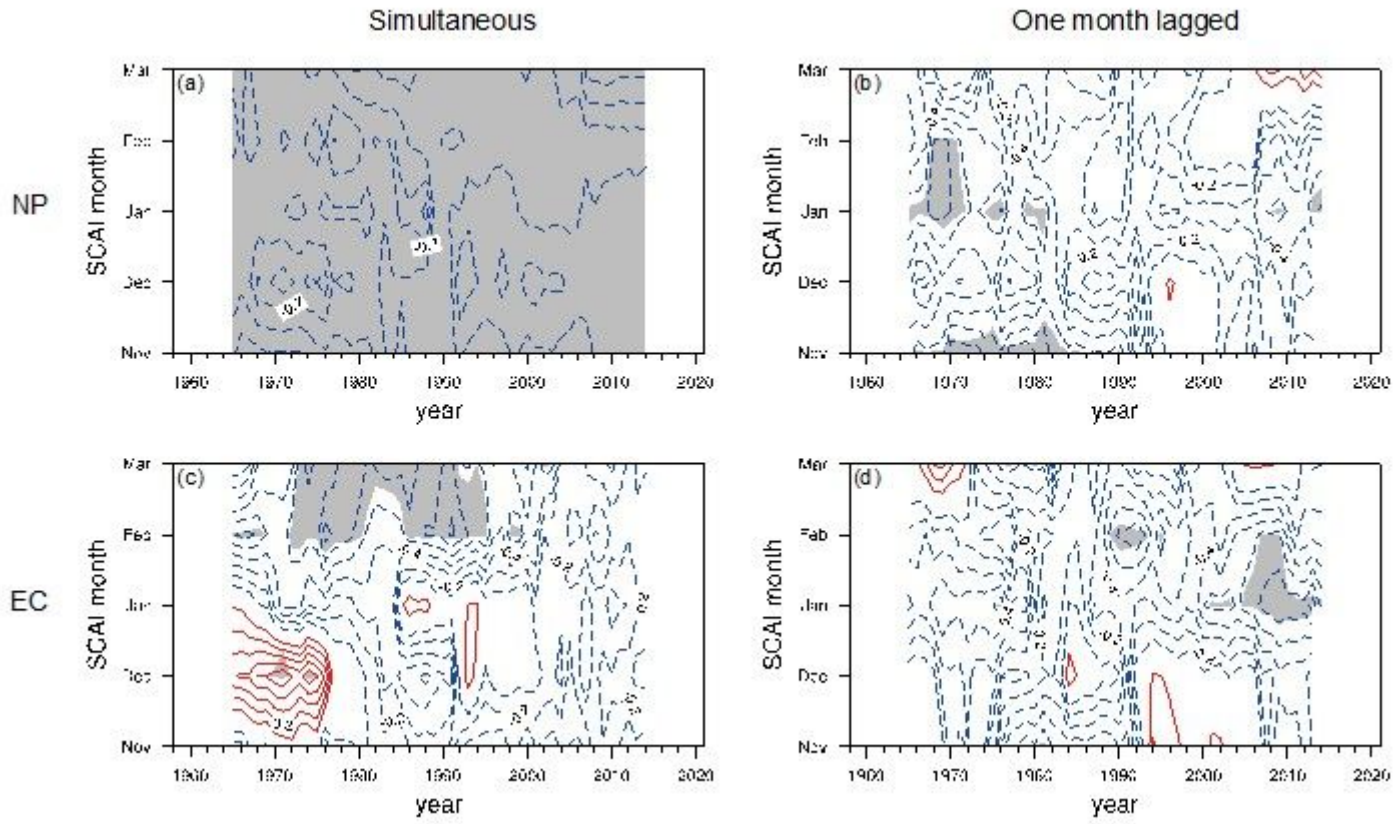

Figure 6

Fifteen-year running correlation coefficients between the monthly SCA indices and (a) simultaneous and (b) one-month-lagged regional mean SAT anomalies over the NP (45-60°N, 70-110°E). (c) and (d) are the same as (a) and (b), but over the EC (25-40°N, 110-120°E) (based on the ERA5 reanalysis dataset). Contour interval is 0.1. Red solid contours and blue dashed contours are the positive and negative coefficients, respectively. Zero lines are omitted. Gray shading indicates the significance at the 95% confidence level

Supplementary Files

This is a list of supplementary files associated with this preprint. Click to download.

- SupplementaryInformation.docx